# Weierstraß–Institut
## für Angewandte Analysis und Stochastik

im Forschungsverbund Berlin e.V.


# Equilibrium thermodynamics of pseudoelasticity and quasiplasticity


Stefan Seelecke



submitted: 22nd December 1995



Weierstraß–Institut
für Angewandte Analysis
und Stochastik
Mohrenstraße 39
D – 10117 Berlin
Germany



Preprint No. 212
Berlin 1995

Edited by
Weierstraß–Institut für Angewandte Analysis und Stochastik (WIAS)
Mohrenstraße 39
D — 10117 Berlin
Germany

Fax: + 49 30 2044975
e–mail (X.400): c=de;a=d400-gw;p=WIAS-BERLIN;s=preprint
e–mail (Internet): preprint@wias-berlin.de

**Abstract**

Motivated by recent experimental results by Glasauer [7], a thermodynamic theory of shape memory alloys is proposed, which includes not only the high temperature - pseudoelastic - behavior but also the low temperature range of quasiplasticity. Due to the occurance of three different phases - austenite and two martensitic variants - several cases of two-phase equilibria and a three-phase equilibrium have to be taken into account. Their relevance is determined by minimization of the total free energy and subsequently illustrated by the construction of phase charts. A special point of interest is the influence of interfacial energy effects on these phase charts, resulting in phenomena like, for example, the apparent violation of Gibbs' phase rule. Furthermore, their role in the hysteretic load-displacement behavior is discussed in the light of the additional quasiplastic case.

# 1 Introduction

Shape memory alloys show a strongly temperature dependent load-displacement behavior, termed *pseudoelastic* at elevated and *quasiplastic* at lower temperatures. A diversity of experimental and theoretical research results can be found, for example, in the various proceedings of the International Conference on Martensitic Transformations (ICOMAT) [16, 5, 19, 17, 15]. For a general overview of the behavior and different approaches to thermodynamic modeling of quasiplasticity and pseudoelasticity, see [13].

In both cases, one observes the occurance of hysteresis loops, connected with phase transitions in the underlying crystal structure. Due to its accessibility in a simple tensile experiment, the pseudoelastic hysteresis has been the subject of detailed investigations for some years now. For example, Xu [11] studied its temperature dependence in the case of *CuZnAl* single crystals, and in [6], Fu found a complex structure of load-deformation paths in the interior of the hysteresis. In a further experiment, he recorded the number of interfaces evolving during the phase transition [9]. These observations have been modeled by Huo and Müller in [6, 9] and [8], who developed a systematic thermodynamic theory of pseudoelasticity.

Only recently, Glasauer [7] performed experiments in the entire tension-compression range, which made it possible to study the complete quasiplastic hysteresis, including its internal structure. In [18], an extension of the existing thermodynamic theory of shape memory alloys is given to account for

these new observations. The main ideas of this work are reviewed in the present paper.

For this purpose, the following section starts with a brief overview of the key aspects of Glasauer's results.

Section 3 then recalls the fundamental concept of equilibrium thermodynamics and provides the constitutive theory necessary to describe phase transitions. Equilibrium conditions are derived, which - in the context of deformation-controlled experiments - lead to the requirement for the total free energy of the specimen to attain a minimum.

This minimization is performed in the first part of section 4. In contrast to pseudoelasticity, the occurance of three phases - austenite and two martensitic variants - gives rise to several possible multi-phase configurations of the body. Their relevance is illustrated by the construction of phase charts, which resemble the temperature-composition phase diagrams of binary alloys. As in that case, they indicate the domain of control parameters - here temperature $T$ and displacement $D$, where the corresponding configurations represent stable equilibrium states. In particular, the influence of interfacial energy on these phase charts is studied. For example, it allows for the existence of three-phase equilibria along line segments instead of confining them to a single point as predicted by the classical Gibbs' phase rule. Moreover, it leads to the observation that the phase deformations no longer coincide with phase boundaries as they do for vanishing interfacial energy. Finally, load-displacement diagrams are constructed, and the comparison of the pseudoelastic and quasiplastic hysteresis loops shows that interfacial energy cannot be the sole ingredient to hysteretic behavior.

# 2 Experimental Observations

In [7], Glasauer has studied the load-deformazion behavior of *CuZnAl* single crystals. With a specially designed device he was able to perform not only tensile experiments, but to enter the compressive range as well. This made it possible to record a complete quasiplastic hysteresis, including the paths in its interior. Fig. 1 shows several such paths, which are the result of unloading upon partial yield or reloading upon partial recovery. Even though the behavior is not as pronounced as in the pseudoelastic case (see [6] for comparison), it shows very similar characteristics. For each internal path, there is a point that indicates the onset of internal yielding or recovery, respectively, and the connection of these points also produces a diagonal line like in the pseudoelastic case.

Fig. 2 - 4 show the results of complete tensile-compressive loading cycles

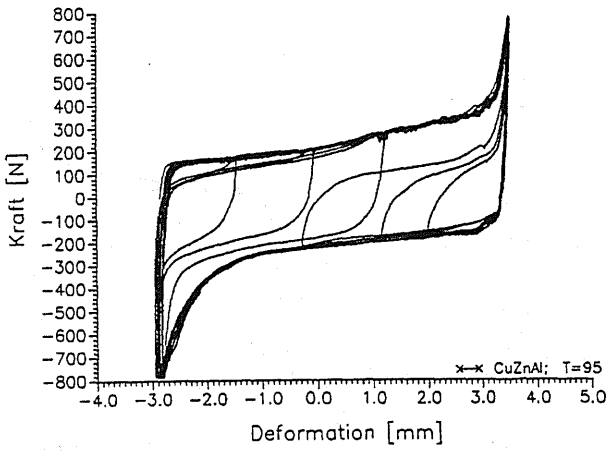


**Figure 1**: *Internal load-deformation paths of the quasiplastic hysteresis in a CuZnAl single crystal*

at different temperatures. Fig. 2 depicts the pseudoelastic behavior at high temperatures with two hysteresis loops, fig. 4 shows the quasiplastic hysteresis, and fig. 3 is recorded at an intermediate temperature, showing the transition between the two extremes.

Observation of the specimen surface reveals that it is necessary to account for at least three phases. The tensile pseudoelastic hysteresis is connected with a load-induced transformation from austenite to a variant of martensite, oriented favorably to the direction of the applied load[1]. During the compressive hysteresis, we observe the formation of a symmetry-related variant, which - under the reversed load - is now sheared to the opposite direction as in the tensile case. The quasiplastic hysteresis turns out to be the consequence of a transformation from one martensitic variant to the other.

Furthermore, it can be observed that all phase transitions proceed by the formation and annihilation of an immense number of alternating layers, thus causing a corresponding number of interfaces between the individual phases. In the pseudoelastic case, this phenomenon has been studied by Fu [9], who counted the number of these interfaces as a function of phase fraction, see fig. 5.

Finally, it is important to note that all reported experiments have been performed quasistatically. In addition to this, only negligibly small relaxation effects have been observed [14], so that we interpret the state in the material as a state of - at least metastable - thermodynamic equilibrium.

[1]For an introduction to the theory of martensitic transformations, see [2, 3, 4] and [20], for example.

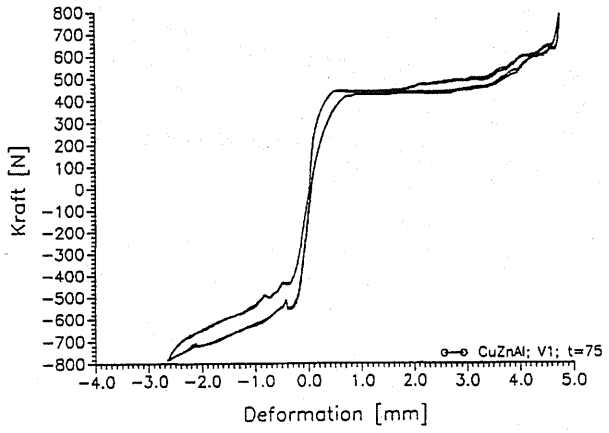


**Figure 2**: *Pseudoelastic behavior of a* CuZnAl *single crystal in tension and compression [7]*

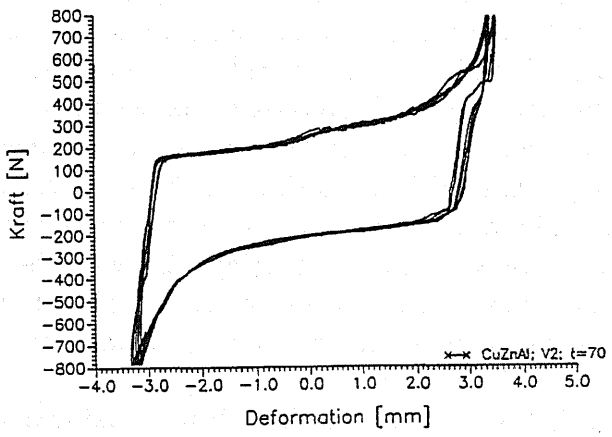


**Figure 3**: *Transition Pseudoelasticity⟷Quasiplasticity*

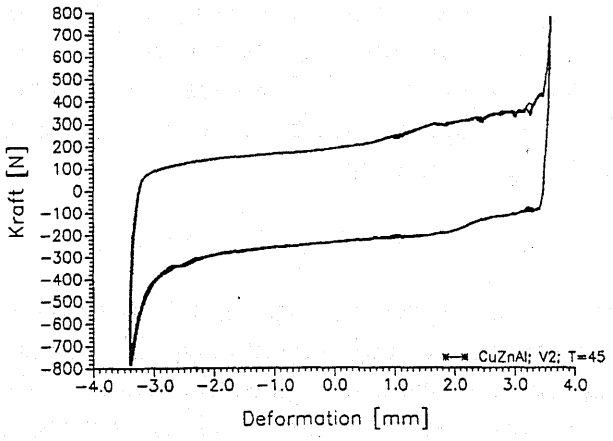


**Figure 4:** *Quasiplastic hysteresis loop [7]*

# 3 Equilibrium Thermodynamics

Application of the first and second law of thermodynamics to a one-dimensional tensile experiment yields the following thermodynamic stability criterion:

$$\frac{d}{dt}(U - T_0 S) \leqq -S\frac{dT_0}{dt} + P\frac{dD}{dt} \,. \tag{1}$$

$U$ and $S$ are internal energy and entropy of the body under consideration. $D$ is the end displacement of the bar, $P$ is the load necessary to maintain it and $T_0$ is the temperature at the surface of the specimen.

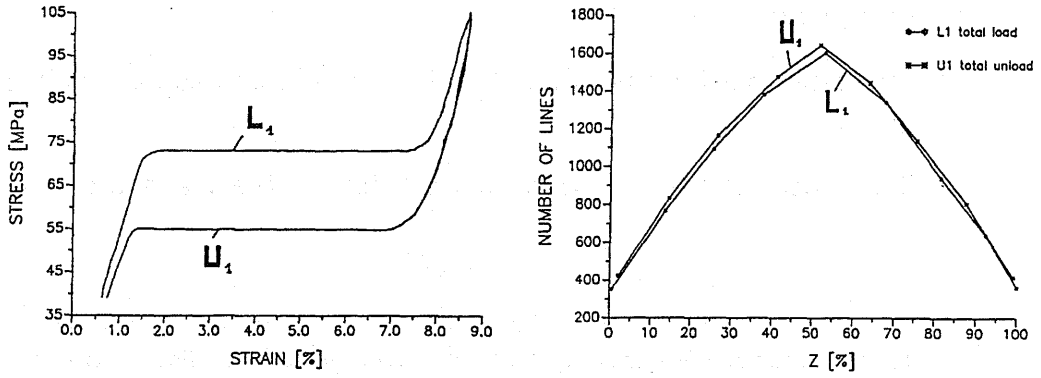


**Figure 5:** *Number of interfaces vs. phase fraction during a complete pseudoelastic hysteresis loop [9]*

Obviously, this criterion is useful if temperature and displacement are the quantities that are controlled in the experiment. In particular, if they are fixed, the combination $U - T_0 S$ decreases with time until it reaches a stationary value in equilibrium, where the equality sign in (1) is valid. This implies the equilibrium condition

$$U - T_0 S \quad \text{to be} \quad \textit{minimal.} \tag{2}$$

It is relevant in a quasistatic experiment, because here, experimental observation suggests that the adjustment of equilibrium is considerably faster than the change in displacement. Thus, the latter is seen by the body as a sequence of constant levels, under which it establishes a corresponding sequence of equilibria.

## 3.1 Availability

For further evaluation of (2), it is necessary to specify the availability $\mathcal{A}_D := U - T_0 S$, which - in the context of this paper - will be subject to the following assumptions:

1. The body is one-dimensional, in particular the displacement vector is of the form $u_i = (u_1(x), 0, 0)$.

2. The only phases occuring are the austenitic phase $A$ and two martensitic phases $M_+$ and $M_-$. These are the oppositely sheared twins of the only variant observed in a uniaxial experiment. In the one-dimensional picture, $M_+$ contributes to an elongation of the bar and $M_-$ to its shortening.

3. The mass density $\rho$ is assumed to be constant and equal for all three phases.

4. The contribution of an individual interface to the availability is given by

   $$\sigma_{\Delta\Gamma} bh.$$

   $\sigma_{\Delta\Gamma}$ is called interfacial energy coefficient between the phases $\Delta$ and $\Gamma$. It is a measurable quantity and - due to crystal symmetry - is the same for combinations $A/M_+$ and $A/M_-$. $b$ and $h$ are thickness and height of the bar, respectively.

Accounting for the fact that the phase transformation proceeds by the formation of alternating layers of different phases, we write the availability as sums over the individual layers and intermediate interfaces:

$$\frac{\mathcal{A}_D}{bh} = \sum_{\Gamma} \sum_{\alpha=1}^{N_\Gamma} \int_{l_\Gamma^\alpha}^{r_\Gamma^\alpha} \rho \left( u_\Gamma - T_0 s_\Gamma \right) dx + \sum_{\Delta \neq \Gamma} N_{\Delta\Gamma} \sigma_{\Delta\Gamma}, \tag{3}$$

$$\text{with } \Gamma, \Delta \in [A, M_+, M_-] .$$

$l_\alpha^\Gamma$ and $r_\alpha^\Gamma$ are the left- and right-hand side coordinates of layer $\alpha$ in phase $\Gamma$. $N_\Gamma$ denotes the total number of layers in this phase, and $N_{\Delta\Gamma}$ is the number of interfaces between $\Delta$ and $\Gamma$. To avoid lenghty notation, a summation over the three phases is introduced which is indicated by the subscript $\Gamma$, and the subscript $\Delta \neq \Gamma$ symbolizes that the corresponding summation is to be performed over all three possibilities of differing indices. Due to the constitutive quantities $u = u(\epsilon, T)$ and $s = s(\epsilon, T)$, $\mathcal{A}_D$ depends on the deformation field $\epsilon(x) := \partial u_1 / \partial x$ and the temperature field $T(x)$ as well as on the distribution of the phases, characterized here by $N_{\Delta\Gamma}, N_\Gamma, l_\alpha^\Gamma$ and $r_\alpha^\Gamma$. It has to be minimized subject to the three constraints

$$L = \sum_{\Gamma} \sum_{\alpha=1}^{N_\Gamma} \int_{l_\Gamma^\alpha}^{r_\Gamma^\alpha} dx , \tag{4}$$

$$D = \sum_{\Gamma} \sum_{\alpha=1}^{N_\Gamma} \int_{l_\Gamma^\alpha}^{r_\Gamma^\alpha} \epsilon(x)\, dx \qquad \text{and} \tag{5}$$

$$0 = \sum_{\Gamma} N_\Gamma - 1 - \sum_{\Delta \neq \Gamma} N_{\Delta\Gamma}. \tag{6}$$

The first condition expresses the fact that the phase arrangement has to take place under fixed length of the bar, while the second one gives the resulting end displacement $D$ as the sum of integrals over the deformation field in each layer. The last condition connects the number of interfaces with the number of layers.

The constraints are incorporated into the functional by Lagrange multipliers so that the subsequent minimization can be performed without con-

straints on the expression

$$\mathcal{A}_D^* = \mathcal{A}_D + \alpha\left(L - \sum_\Gamma \sum_{\alpha=1}^{N_\Gamma} \int_{l_\Gamma^\alpha}^{r_\Gamma^\alpha} dx\right) + \lambda\left(D - \sum_\Gamma \sum_{\alpha=1}^{N_\Gamma} \int_{l_\Gamma^\alpha}^{r_\Gamma^\alpha} \epsilon(x)\, dx\right) + \gamma\left(\sum_\Gamma N_\Gamma - 1 - \sum_{\Delta\neq\Gamma} N_{\Delta\Gamma}\right). \tag{7}$$

$\alpha, \lambda$ and $\gamma$ are the Langrange multipliers mentioned above.

## 3.2 Equilibrium Conditions I

From (7) follows the necessary condition for equilibrium

$$\delta\mathcal{A}_D^* = 0\,, \tag{8}$$

which is evaluated in two steps. First, the variation with respect to the temperature field $T(x)$ and the deformation field $\epsilon(x)$ gives[2]

$$\left(\frac{\partial u_\Gamma}{\partial \epsilon}\right)_T - T_0\left(\frac{\partial s_\Gamma}{\partial \epsilon}\right)_T - \frac{\lambda}{\rho b h} = 0 \qquad \text{and} \tag{9}$$

$$\left(\frac{\partial u_\Gamma}{\partial T}\right)_\epsilon - T_0\left(\frac{\partial s_\Gamma}{\partial T}\right)_\epsilon = 0\,. \tag{10}$$

(9) and (10) represent three equations each, valid in every single layer of phase $\Gamma$.

Assuming local equilibrium, one can further exploit (9) and (10), using the Gibbs equation

$$Tds = du - \frac{\sigma}{\rho} d\epsilon\,, \tag{11}$$

where $\sigma$ is the 11-component of the stress tensor. Its application yields the conditions for thermal and mechanical equilibrium

$$T(x) = T_0 \quad \text{and} \quad \sigma(x) = \frac{\lambda}{bh}\,, \tag{12}$$

requiring temperature and stress to be constant throughout the bar. Moreover, if $(12)_2$ is applied to the end of the bar, $\lambda$ can be identified as the load $P$.

The resulting deformation field, however, cannot be calculated without further knowledge of the constitutive functions $u_\Gamma(\epsilon, T)$ and $s_\Gamma(\epsilon, T)$, or -

[2]For a detailed discussion of the derivation, see ??.

with $(12)_1$ - the free energy density $f_\Gamma(\epsilon, T)$. Additionally, the insertion of these quantities considerably simplifies the evaluation of the remaining conditions for phase equilibrium. For this reason, the following section derives an expression for the free energy density suitable for the description of phase transitions.

## 3.3 A Model Free Energy Density for Shape Memory Behavior

The calculation of the free energy density again relies on the local validity of the Gibbs equation. The simplest case is the one of a linearly elastic material without thermal expansion obeying a generalized Hooke's law:

$$\sigma_\Gamma = E(\epsilon_\Gamma - \epsilon_\Gamma^*). \tag{13}$$

Here, the Young's modulus $E$ is the same for each phase and $\epsilon_\Gamma^*$ is the known stress-free transformation strain

$$\epsilon_\Gamma^* = \begin{cases} \epsilon^T & (\text{martensite } M_+) \\ 0 & (\text{austenite } A) \\ -\epsilon^T & (\text{martensite } M_-) \end{cases} . \tag{14}$$

If also the specific heat $c$ is taken to be the same for each phase and independent of temperature, the Gibbs equation in the form

$$df_\Gamma = -s_\Gamma dT + \frac{\sigma_\Gamma}{\rho} d\epsilon \tag{15}$$

can be integrated to yield

$$f_\Gamma(\epsilon, T) = \Theta_\Gamma(T) + \frac{1}{2\rho} E(\epsilon - \epsilon_\Gamma^*)^2 \tag{16}$$

with

$$\Theta_\Gamma(T) = -cT \ln \frac{T}{T_R} + c(T - T_R) - s_\Gamma^R (T - T_R) . \tag{17}$$

Thus, the free energy is given by a parabolic dependence on strain, shifted along the $\epsilon$-axis according to the phase under consideration. The functions $\Theta_\Gamma(T)$ must be such that martensite is stable at low temperatures and austenite at high temperatures. They are adjusted by a proper choice of the entropy constants $s_\Gamma^R$, which is the reason that this behavior is termed *entropic stabilization* of austenite. Note that, due to crystal symmetry, $s_+^R = s_-^R$.

Figure 6 shows the free energy density for several different temperatures. The intermediate diagram, where all three minima are at the same height, refers to the case $T_2 = T_R$, the temperature of the reference state.

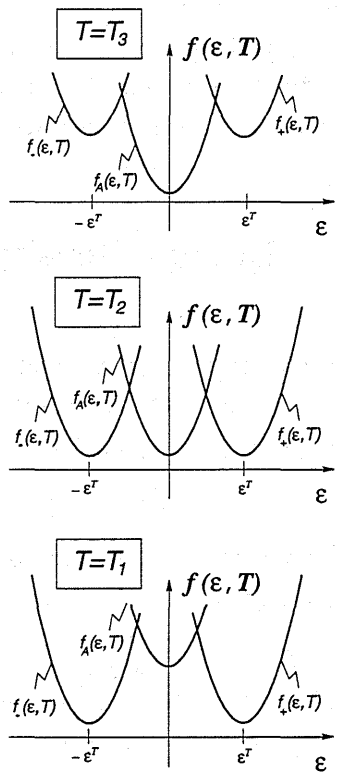


**Figure 6**: *Free energy density vs. strain for three characteristic temperatures*

## 3.4 Equilibrium Conditions II

From the condition $(12)_2$ , $\sigma(x) = const.$, it follows with (13) that there are three different solutions for the deformation field. Depending on the phase at hand, it takes on the values $\epsilon(x) = \epsilon_\Gamma$, being constant in each layer. This circumstance turns $\mathcal{A}_D^*$ into a function of the discrete variables $\epsilon_\Gamma$ which, because of $T(x) = T_0$, has become the total free energy $F$, reading

$$\frac{F}{bh} = \sum_\Gamma \rho f_\Gamma(\epsilon_\Gamma, T) \sum_{\alpha=1}^{N_\Gamma} \int_{l_\Gamma^\alpha}^{r_\Gamma^\alpha} dx + \sum_{\Delta \neq \Gamma} N_{\Delta\Gamma} \sigma_{\Delta\Gamma} \,. \tag{18}$$

Note that thus the explicit dependence on $N_\Gamma, l_\Gamma^\alpha$ and $r_\Gamma^\alpha$ has vanished. Instead, upon introduction of specific quantitites, the phase distribution is solely given by the phase fractions

$$z_\Gamma := \frac{1}{L} \sum_{\alpha=1}^{N_\Gamma} \int_{l_\Gamma^\alpha}^{r_\Gamma^\alpha} dx \,, \tag{19}$$

and the specific free energy reads

$$f := \frac{F}{m} = \sum_{\Gamma} z_\Gamma f_\Gamma\left(\epsilon_\Gamma, T\right) + \sum_{\Delta \neq \Gamma} N_{\Delta\Gamma} \frac{\sigma_{\Delta\Gamma}}{\rho L} . \tag{20}$$

Insertion of the free energy density (16) also modifies the constraints to

$$1 = \sum_{\Gamma} z_\Gamma \quad \text{and} \tag{21}$$

$$\frac{D}{L} = \sum_{\Gamma} z_\Gamma \epsilon_\Gamma . \tag{22}$$

The third condition is rendered superflous, because $N_\Gamma$ does not appear among the list of variables anymore.

A final remark has to be given with respect to the dependence on the number of interfaces $N_{\Delta\Gamma}$. According to the present model, the first sum in (20), representing the bulk contribution of the phases, depends only on the phase fraction regardless of the number of layers and thus the number of interfaces. Upon minimization of $f$ with respect to $N_{\Delta\Gamma}$, this leads to the circumstance that the number of interfaces will always take on the values $N_{\Delta\Gamma} = 1$ if the phases $\Delta$ and $\Gamma$ are present. As this is not in good agreement with experimental observations, $N_{\Delta\Gamma}$ are dropped from the list of variables and rather interpreted as constitutive quantities, for which an ansatz of the form

$$N_{\Delta\Gamma} = C_{\Delta\Gamma} z_\Delta z_\Gamma \qquad \text{(no summation)} \tag{23}$$

is made. This goes back to a proposition originally made by Müller [10]. It links the number of interfaces to the phase fraction in such a way that they are zero for the case of pure phase $\Delta$ or $\Gamma$, respectively, and run through a maximum inbetween. This corresponds to the results of figure 5, which also allow for the determination of the proportionality coefficients $C_{\Delta\Gamma}$.

As a conclusion of the foregoing results, the possible equilibrium states of a shape memory bar are obtained from the minimization of the following augmented free energy function

$$\begin{aligned} f^* = \sum_{\Gamma} z_\Gamma f_\Gamma\left(\epsilon_\Gamma, T\right) + \sum_{\Delta \neq \Gamma} C_{\Delta\Gamma} z_\Delta z_\Gamma \frac{\sigma_{\Delta\Gamma}}{\rho L} + \alpha \left(1 - \sum_{\Gamma} z_\Gamma\right) \\ + \lambda \left(\frac{D}{L} - \sum_{\Gamma} z_\Gamma \epsilon_\Gamma\right) . \end{aligned} \tag{24}$$

# 4 Equilibrium States

For the subsequent treatment, it is useful to introduce the dimensionless quantities

$$\begin{aligned} \tilde{\epsilon}_\Gamma &:= \frac{\epsilon_\Gamma}{\epsilon^T}\,, \\ \tilde{D} &:= \frac{D}{L\epsilon^T} \qquad \text{and} \end{aligned} \tag{25}$$

$$\tilde{f} := \frac{f}{\frac{E}{\rho}\left(\epsilon^T\right)^2} = \sum_\Gamma z_\Gamma \tilde{f}_\Gamma \quad \text{with} \quad \tilde{f}_\Gamma := \tilde{\Theta}_\Gamma\left(\tilde{T}\right) + \tfrac{1}{2}\left(\tilde{\epsilon}_\Gamma - \tilde{\epsilon}_\Gamma^*\right)^2 \,, \tag{26}$$

$$\text{where} \qquad \tilde{\epsilon}_\Gamma^* := \begin{cases} 1 & (\text{martensite } M_+) \\ 0 & (\text{austenite } A) \\ -1 & (\text{martensite } M_-) \end{cases} . \tag{27}$$

$A_{\Delta\Gamma}$ denote the dimensionless interfacial energy coefficients with

$$A_{\Delta\Gamma} := \frac{\sigma_{\Delta\Gamma} C_{\Delta\Gamma}}{EL\left(\epsilon^T\right)^2}\,, \tag{28}$$

and the augmented free energy reads

$$\tilde{f}^* := \sum_\Gamma z_\Gamma \tilde{f}_\Gamma + \sum_{\Delta\neq\Gamma} A_{\Delta\Gamma} z_\Delta z_\Gamma + \tilde{\alpha}\left(1 - \sum_\Gamma z_\Gamma\right) + \tilde{\lambda}\left(\tilde{D} - \sum_\Gamma z_\Gamma \epsilon_\Gamma\right) , \tag{29}$$

with $\tilde{\alpha}$ and $\tilde{\lambda}$ being the dimensionless Lagrange multipliers

$$\begin{aligned} \tilde{\lambda} &:= \frac{\lambda}{E\epsilon^T bh} \qquad \text{and} \\ \tilde{\alpha} &:= \frac{\alpha}{E\left(\epsilon^T\right)^2}\,. \end{aligned} \tag{30}$$

## 4.1 Necessary Conditions for Equilibrium

The resulting necessary conditions for equilibrium read

$$\begin{aligned} 0 &= \left(\frac{\partial \tilde{f}_A}{\partial \tilde{\epsilon}_A}\right)_T - \tilde{\lambda} = \tilde{\epsilon}_A - \tilde{\lambda}\,, \\ 0 &= \left(\frac{\partial \tilde{f}_+}{\partial \tilde{\epsilon}_+}\right)_T - \tilde{\lambda} = (\tilde{\epsilon}_+ - 1) - \tilde{\lambda}\,, \\ 0 &= \left(\frac{\partial \tilde{f}_-}{\partial \tilde{\epsilon}_-}\right)_T - \tilde{\lambda} = (\tilde{\epsilon}_- + 1) - \tilde{\lambda}\,, \end{aligned}$$

$$
\begin{aligned}
0 &= \left(\frac{\partial \tilde{f}^*}{\partial z_A}\right)_{T,\epsilon_\Gamma,z_\Gamma \neq z_A} = \tilde{f}_A - \tilde{\alpha} - \tilde{\lambda}\tilde{\epsilon}_A + A_{AM}\left(z_+ + z_-\right), && (31)\\
0 &= \left(\frac{\partial \tilde{f}^*}{\partial z_+}\right)_{T,\epsilon_\Gamma,z_\Gamma \neq z_+} = \tilde{f}_+ - \tilde{\alpha} - \tilde{\lambda}\epsilon_+ + A_{AM} z_A + A_{+-} z_-, &&\\
0 &= \left(\frac{\partial \tilde{f}^*}{\partial z_-}\right)_{T,\epsilon_\Gamma,z_\Gamma \neq z_-} = \tilde{f}_- - \tilde{\alpha} - \tilde{\lambda}\epsilon_- + A_{AM} z_A + A_{+-} z_+, &&\\
1 &= z_A + z_+ + z_- && \text{and}\\
\tilde{D} &= z_A\tilde{\epsilon}_A + z_+\tilde{\epsilon}_+ + z_-\tilde{\epsilon}_- . &&
\end{aligned}
$$

In $(31)_{1,2,3}$, the first three equations represent the conditions for mechanical equilibrium, while $(31)_{4,5,6}$ is the one-dimensional form of those for phase equilibrium. Together with the last two equations - representing the constraints - (31) is a system for the determination of the unknown deformation in each phase, its phase fraction and the two Lagrange multipliers. Note that thermal equilibrium is already taken into account by replacing the availability by the free energy.

So far, the entire treatment assumed equilibrium among all three phases. Even though this is the general case, there are also the cases of two-phase equilibrium or single-phase existence, which need to be taken into account. Altogether, there are seven different configurations for the body, which will be discussed in a systematic manner as special cases of the general system (31).

### 4.1.1 Single-phase existence

Austenite *A*: The martensite phase fractions are identically zero, $z_+ = z_- = 0$, and the relevant equations for the evaluation are $(31)_{1,4,7,8}$. From $(31)_7$, it follows

$$z_A = 1 \tag{32}$$

[3]and, from $(31)_8$,

$$\epsilon_A = D . \tag{33}$$

With $(31)_1$, one concludes

$$\lambda = D , \tag{34}$$

[3]For readability's sake, the tildes have been omitted again so that from here on all quantities are understood to be dimensionless.

and due to $(31)_4$, it is possible to identify

$$\alpha = f_A - \sigma\epsilon_A = g_A \tag{35}$$

as the free enthalpy. The free energy $f$ finally reads

$$f = f_A(\epsilon_A, T) = \frac{1}{2}D^2 + \Theta_A(T) = f(D,T) \ . \tag{36}$$

**Martensite $M_+$ or $M_-$:** In this case, the following phase fractions vanish, $z_A = z_- = 0$ or $z_A = z_+ = 0$, respectively. The evaluation relies on $(31)_{2,5,7,8}$ or $(31)_{3,6,7,8}$. In analogy to the previous case, $(31)_7$ yields

$$z_\pm = 1 \,, \tag{37}$$

and $(31)_8$ gives

$$\epsilon_\pm = D \ . \tag{38}$$

From $(31)_2$, it follows

$$\lambda = D \mp 1 \,, \tag{39}$$

and due to $(31)_5$, it is again possible to identify

$$\alpha = f_\pm - \sigma\epsilon_\pm = g_\pm \ . \tag{40}$$

The upper sign is valid for the case "$M_+$" and the lower one for "$M_-$". As before, the free energy $f$ depends on $D$ and $T$, reading

$$f = f_\pm(\epsilon_\pm, T) = \frac{1}{2}(D \mp 1)^2 + \Theta_M(T) = f(D,T) \ . \tag{41}$$

### 4.1.2 Two-phase Coexistence

**$M_+$ and $M_-$:** Here, the austenite phase fraction vanishes, $z_A = 0$, and $(31)_{2,3,5,6,7,8}$ are the relevant equations for this case. From $(31)_{2,3}$, one deducts

$$\epsilon_+ - \epsilon_- = 2, \tag{42}$$

from which follows, together with $(31)_5$ - $(31)_6$ and $(31)_{7,8}$,

$$\lambda = \frac{1}{2}A_{+-}(1 - D + \epsilon_-) \ . \tag{43}$$

The phase deformation as well as the Lagrange multiplier $\lambda$ are determined by (43) and $(31)_{2,3}$ to give

$$\epsilon_+ = 1 - \frac{\frac{1}{2}A_{+-}}{1-\frac{1}{2}A_{+-}}D\,, \tag{44}$$

$$\epsilon_- = -1 - \frac{\frac{1}{2}A_{+-}}{1-\frac{1}{2}A_{+-}}D \qquad \text{and} \tag{45}$$

$$\lambda = -\frac{\frac{1}{2}A_{+-}}{1-\frac{1}{2}A_{+-}}D\,. \tag{46}$$

From $(31)_{7,8}$, the phase fractions can be calculated,

$$z_+ = \frac{D-\epsilon_-}{\epsilon_+-\epsilon_-} = \frac{1}{2}\left(1+\frac{D}{1-\frac{1}{2}A_{+-}}\right) \qquad \text{as well as} \tag{47}$$

$$z_- = \frac{\epsilon_+-D}{\epsilon_+-\epsilon_-} = \frac{1}{2}\left(1-\frac{D}{1-\frac{1}{2}A_{+-}}\right)\,, \tag{48}$$

and from $(31)_{5,6}$, one obtains the other Lagrange multiplier

$$\alpha = g_+ + A_{+-}z_+ = g_- + A_{+-}z_-\,. \tag{49}$$

Finally, the free energy of the mixture reads

$$\begin{aligned} f &= z_+ f_+(\epsilon,T) + z_- f_-(\epsilon,T) + A_{+-}z_+z_- = \\ &= \frac{1}{2}(\epsilon_-+1)^2 + \Theta_M(T) + A_{+-}z_+(1-z_+)\,. \end{aligned} \tag{50}$$

*Range of admissibility:* From the condition

$$0 < z_+ < 1\,,$$

it follows with $A_{+-} < 2$ that this case is only admissible , when - independent of temperature $T$ - the control parameter $D$ is in the range

$$-1+\frac{1}{2}A_{+-} < D < 1-\frac{1}{2}A_{+-}\,. \tag{51}$$

**$A$ and $M_+$ or $A$ and $M_-$:** This case is characterized by $z_- = 0$ or $z_+ = 0$, and the relevant equations are $(31)_{1,2,4,5,7,8}$ or $(31)_{1,3,4,6,7,8}$, respectively. From $(31)_{1,2}$ or $(31)_{1,3}$, one calculates the relation between the phase deformations

$$\epsilon_A - \epsilon_\pm = \mp 1\,, \tag{52}$$

and with $(31)_4$ - $(31)_{5,6}$ and $(31)_{7,8}$ it is possible to identify $\lambda$ as

$$\lambda = \frac{\pm B(T) \pm A_{AM}(1 \mp 2D)}{1 - 2A_{AM}} \tag{53}$$

with

$$B(T) := \Theta_M(T) - \Theta_A(T) \ . \tag{54}$$

Again, the upper sign is valid for "$M_+$" and the lower one for "$M_-$". $(31)_{1,2,3}$ then yield the phase deformations

$$\epsilon_A = \frac{\pm B(T) \pm A_{AM}(1 \mp 2D)}{1 - 2A_{AM}} \quad \text{and} \tag{55}$$

$$\epsilon_\pm = \pm 1 + \frac{\pm B(T) \pm A_{AM}(1 \mp 2D)}{1 - 2A_{AM}} \tag{56}$$

as well as - due to $(31)_{7,8}$ - the phase fractions

$$z_A = \frac{\epsilon_\pm - D}{\epsilon_\pm - \epsilon_A} = 1 - \frac{\pm D - B(T) - A_{AM}}{1 - 2A_{AM}} \quad \text{and} \tag{57}$$

$$z_\pm = \frac{D - \epsilon_A}{\epsilon_\pm - \epsilon_A} = \frac{\pm D - B(T) - A_{AM}}{1 - 2A_{AM}} \ . \tag{58}$$

$(31)_{5,6}$ serve to compute the Lagrange multiplier $\alpha$:

$$\alpha = g_A + A_{AM} z_\pm = g_\pm + A_{AM} z_A \ . \tag{59}$$

Finally, the free energy follows as

$$\begin{aligned} f &= z_A f_A(\epsilon, T) + z_\pm f_\pm(\epsilon, T) + A_{AM} z_A z_\pm = \\ &= f_A(\epsilon, T) + z_\pm [f_\pm(\epsilon, T) - f_A(\epsilon, T)] + A_{AM} z_A z_\pm = \\ &= \frac{1}{2}\epsilon_A^2 + \Theta_A(T) + z_\pm [B(T) + A_{AM}(1 - z_\pm)] \ . \end{aligned} \tag{60}$$

*Range of admissibility:* The admissibility of this case is limited to

$$\begin{aligned} B(T) \quad &< \quad D \quad < \quad 1 + B(T) - A_{AM} \qquad \text{for } A/M_+ \text{ or} \\ -1 - B(T) + A_{AM} \quad &< \quad D \quad < \quad -B(T) - A_{AM} \qquad \text{for } A/M_- \ , \end{aligned} \tag{61}$$

assuming $A_{AM} < 1/2$ .

### 4.1.3 Three-phase Coexistence

The evaluation of the three-phase case requires all eight equations. $(31)_{1,2,3}$ give

$$\epsilon_A = \epsilon_+ - 1 = \epsilon_- + 1 \,. \tag{62}$$

and from $(31)_5$ - $(31)_6$, it follows

$$\lambda = -\frac{1}{2} A_{+-} \left( z_+ - z_- \right) \,, \tag{63}$$

or - together with $(31)_1$ and $(31)_{7,8}$ -

$$\lambda = -\frac{\frac{1}{2}A_{+-}}{1 - \frac{1}{2}A_{+-}} D \,. \tag{64}$$

The phase deformations are calculated from $(31)_{1,2,3}$ to be

$$\begin{aligned} \epsilon_A &= -\frac{\frac{1}{2}A_{+-}}{1 - \frac{1}{2}A_{+-}} D \,, \\ \epsilon_+ &= 1 - \frac{\frac{1}{2}A_{+-}}{1 - \frac{1}{2}A_{+-}} D \qquad \text{and} \\ \epsilon_- &= -1 + \frac{\frac{1}{2}A_{+-}}{1 - \frac{1}{2}A_{+-}} D \,, \end{aligned} \tag{65}$$

and from $(31)_{4,5,6}$, one obtains

$$\alpha = g_A + A_{AM} \left( z_+ + z_- \right) = g_+ + A_{AM} z_A + A_{+-} z_- = g_- + A_{AM} z_A + A_{+-} z_+ \,. \tag{66}$$

The phase fractions $z_A, z_+$ and $z_-$ are determined from $(31)_4$ - $(31)_5$, $(31)_5$ - $(31)_6$ and $(31)_{7,8}$:

$$z_+ = \frac{1}{2} \left[ \frac{B\left(T\right) + A_{AM}}{2A_{AM} - \frac{1}{2}A_{+-}} + \frac{1}{1 - \frac{1}{2}A_{+-}} D \right] \,, \tag{67}$$

$$z_- = \frac{1}{2} \left[ \frac{B\left(T\right) + A_{AM}}{2A_{AM} - \frac{1}{2}A_{+-}} - \frac{1}{1 - \frac{1}{2}A_{+-}} D \right] \qquad \text{and} \tag{68}$$

$$z_A = 1 - \frac{B\left(T\right) + A_{AM}}{2A_{AM} - \frac{1}{2}A_{+-}} \,. \tag{69}$$

Insertion into the free energy finally gives

$$f = z_A f_A + z_+ f_+ + z_- f_- + A_{AM} z_A \left( z_+ + z_- \right) + A_{+-} z_+ z_- =$$

$$
\begin{aligned}
&= f_A + z_+ [f_+ - f_A] + z_- [f_- - f_A] + \\
&\quad + A_{AM} (1 - z_+ - z_-) (z_+ + z_-) + A_{+-} z_+ z_- \\
&= \frac{1}{2}\epsilon_A^2 + \Theta_A (T) + (z_+ + z_-) [B (T) + A_{AM} (1 - z_+ - z_-)] + \\
&\quad + A_{+-} z_+ z_- \, . \qquad (70)
\end{aligned}
$$

*Range of admissibility:* With $A_{AM} > A_{+-}/4$, the equation for $z_A$ (69) restricts the admissible temperatures to

$$
-A_{AM} < B (T) < A_{AM} - \frac{1}{2} A_{+-} \, . \qquad (71)
$$

This, together with $z_+ > 0$ und $z_- > 0$, then limits the end displacement $D$ to the range:

$$
-[B (T) + A_{AM}] \frac{1 - \frac{1}{2} A_{+-}}{2A_{AM} - \frac{1}{2} A_{+-}} < D < [B (T) + A_{AM}] \frac{1 - \frac{1}{2} A_{+-}}{2A_{AM} - \frac{1}{2} A_{+-}} \, . \qquad (72)
$$

From the previous results, the values of $\epsilon_\Gamma$, $z_\Gamma$, $\alpha$ and $\lambda$ are known for each of the seven cases. However, they follow from the necessary conditions only, and the question remains, which of the possible configurations is the one prevailing in equilibrium.

## 4.2 Sufficient Conditions for Equilibrium

To answer this question, it is necessary to determine the configuration which - for a given set of control parameters $(D, T)$ - actually minimizes the free energy. In the case of vanishing interfacial energy, illustrative methods are provided by the well-known Maxwell construction and the common tangent construction. Unfortunately, these constructions are no longer applicable in the general case. The tangents to the free energy at the points $\epsilon_\Gamma$ are not equal to the slope of the line given by the difference quotient anymore. Instead, they differ from each other by an amount that depends on the actual value of $D$, which renders the method impracticable. To circumvent this inconvenience, a variant of the Maxwell construction has been employed by Müller and Bornert [1] for the treatment of the pseudoelastic phase transition. However, this method involves a cumbersome measuring of areas, and moreover, the Maxwell construction does not provide any evidence on the minimality characteristic of the considered case. As the latter is not a problem in pseudoelasticity, it is crucial for cases with more than two possible phases involved.

For this reason, the present paper follows a different path. With the knowledge of the individual free energies from the previous section, it is possible to *calculate* the transition points from one solution to another. Graphical methods are only employed in order to illustrate the behavior.

Figures 7 - 10 show plots of the seven total free energies[4] as functions of the end displacement $D$ for several characteristic temperatures, represented by the function $B(T) := \Theta_M(T) - \Theta_A(T)$. The solid lines denote the single phases, while the phase mixtures can be identified by the following table:

| | |
|---|---|
| ····· | $A/M_+/M_-$ |
| −·−·− | $A/M_\pm$ |
| − − − | $M_+/M_-$ |

The underlying values for the interfacial energy coefficients are $A_{AM} = 0.1$ and $A_{+-} = 1/10 A_{AM} = 0.01$.[5] Their ratio reflects the fact that the interfacial energy arises because of a misfit at the phase boundaries. Due to the differing lattice parameters between austenite and martensite, the misfit of such a combination is considerably larger than the one of two martensite variants.

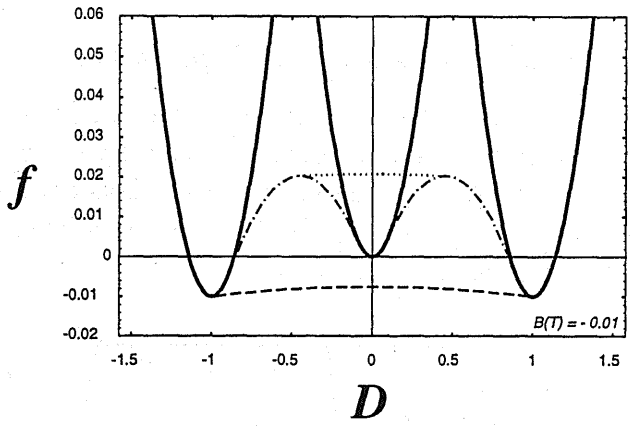


**Figure 7**: *Free energies for the seven possible phase configuration at low temperatures*

Figure 7 shows the free energies at low temperatures. Differing from the case without interfacial energy, where - according to the common tangent

[4]Note that despite the similarity to figure 6, the following diagrams do *not* show the mass density of free energy, which is a local quantity depending on $\epsilon_\Gamma$ and $T$. Rather they illustrate the global free energy of the bar as a function of $D$ an $T$, which is the quantity to attain a minimum.

[5]The order of magnitude of these coefficients has been chosen for illustrative purposes only. A realistic estimate based on interfacial energy coefficients for coherent interfaces produces a value for $A_{AM} \approx 2 \cdot 10^{-6}$.

construction - they are given by straight lines, the free energies of the phase mixtures here are concave parabolae. Nevertheless, for $-1 + A_{+-}/2 < D < 1 - A_{+-}/2$, the mixture $M_+/M_-$ represents the stable equilibrium, minimizing the total free energy in this range.

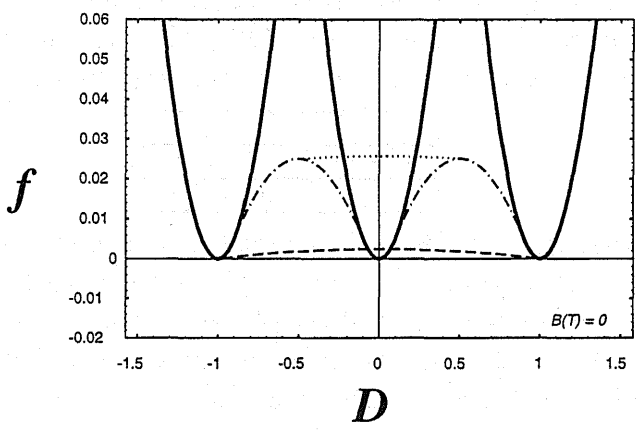


**Figure 8**: *Free energies for the case of equal height of the three minima*

In figure 8, the case of equal height of all three minima is depicted. It is interesting to note that, for small values of $|D|$, it is energetically favorable for the bar to exist as one purely austenitic phase. This is due to the interfacial energy which has to be "paid" in the $M_+/M_-$-case because, in this range, the number of interfaces is maximal.

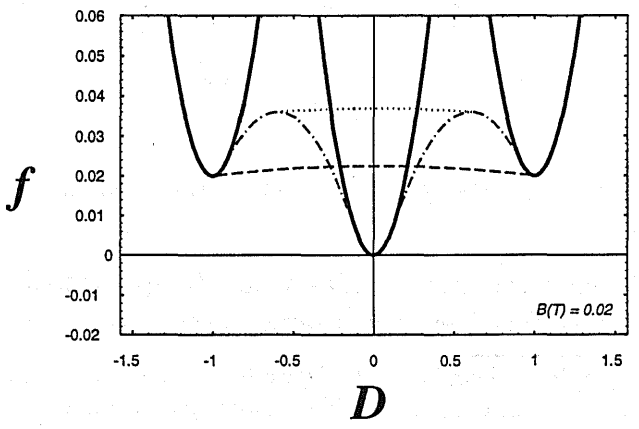


**Figure 9**: *Free energies for the case of intermediate temperatures*

For $B(T) = 0.02$ (figure 9), yet another case can be observed. In a

small intermediate range of $|D|$, the body forms a mixture $A/M_+$ or $A/M_-$, respectively. However, with increasing end displacement and thus inreasing number of interfaces forming, this becomes unfavorable again compared to the case $M_+/M_-$.

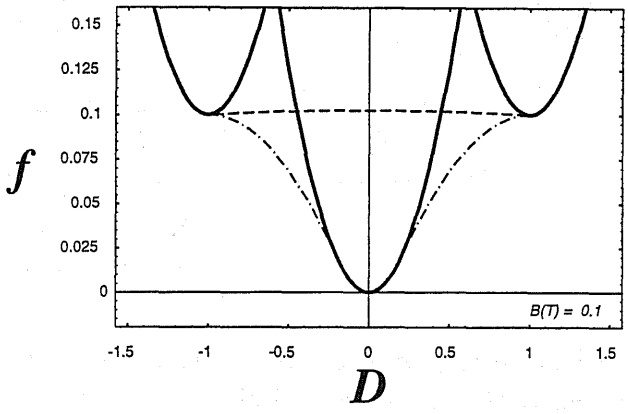


**Figure 10:** *Free energies for the case high temperatures*

For high temperatures, there are no more values of $D$ for which the mixture $M_+/M_-$ minimizes the free energy, see figure 10. This is the temperature range of purely pseudoelastic behavior. Note that the plotted case also marks the disappearance of the three-phase mixture, which for no temperature represented the state of stable equilibrium, though.

## 4.3 Phase Charts

From the previous section, the energy minimizing configurations can be determined for an arbitrary set of $D$ and $T$. For a convenient overview, it is useful to assemble these results in the form of a map. This map is constructed by determination of those values of $D$ which - for a given temperature - indicate the equality of the free energy of two phase configurations. The lines thus entered into the map are called phase boundaries.

Of particular interest in the context of this paper is the influence of interfacial energy on these phase boundaries, and to study this, at first the case of zero interfacial energy is presented in figure 11.

From here, the regions in $(D,T)$-space can be extracted, where the individual phase configurations represent the stable equilibrium state. At low temperatures $(B(T) < 0)$, the pure martensite phases or a mixture of them are relevant, and at higher temperatures - depending on the value of $D$ -

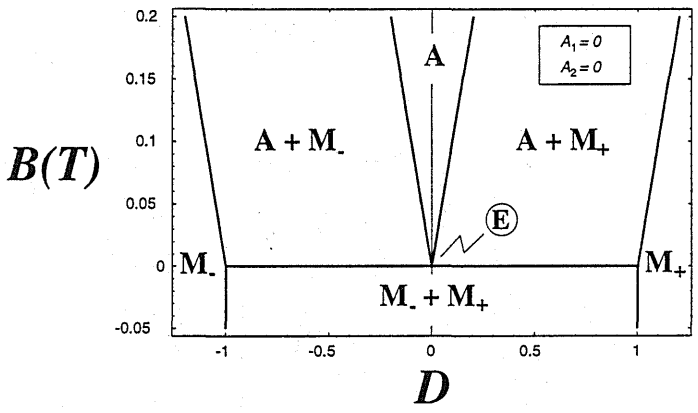


**Figure 11:** *Phase chart for a shape memory bar in a tensile experiment witout the influence of interfacial energies.*

either pure austenite or an austenite-martensite mixture becomes important. For $D = 0$ and $B(T) = 0$, there exists a point **E** which strongly resembles the eutectoidal point in the composition-temperature phase diagram of a binary alloy with a miscibility gap. This, together with the overall resemblence of the two diagrams, gives rise to a detailed discussion of the analogy in the thermodynamic treatment, which will be presented in a forthcoming paper. Note, however, that even though it is termed *alloy*, the shape memory bar in the context of this paper is treated as a one-component material. This is because it does not change composition in a tensile experiment and we are only interested in its deformation-temperature behavior. To avoid confusion, the paper always speaks about phase *charts* instead of phase *diagrams* in this context.

Figure 12 shows the influence of interfacial energy for combinations $A/M_{\pm}$. It is evident that all neighboring regions expand at the expense of the one penalized by the interfacial energy. Moreover, the point **E** from figure 11, allowing for a direct transition from austenite to martensite, has developed into a curved line.

This feature calls for a discussion because, at first glance, it seems to pose a violation of Gibbs' phase rule. This rule states that, for a one-component material in three phases, there should be no degree of freedom, thus confining the possible equilibrium states to a point. The explanation for this apparent contradiction is due to the fact that the phase rule in its original form has been derived from the equilibrium condition without interfacial energy. This condition requires the continuity of the chemical potential at each interface

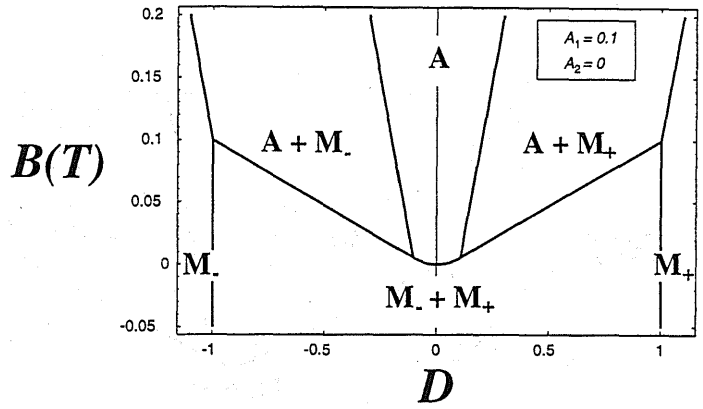


**Figure 12**: *Phase chart for a shape memory bar in a tensile experiment with interfacial energy only between $A/M_\pm$ ($A_1 = 0.1, A_2 = 0$).*

or - in the case of a one-component material - the continuity of the free enthalpy. Inspection of (59) for example reveals that this is no longer valid in the presence of interfacial energy. Instead, the continuity of the combination

$$g_A + A_{AM} z_\pm = g_\pm + A_{AM} z_A$$

is required so that the additional quantities $z_\Gamma$ enter the condition. In equilibrium, these have been computed as functions of $D$ so that the phase rule can still be considered valid, only now for every prescribed value of $D$. Thus, in the presence of interfacial energy, three-phase equilibrium is not confined to a point in the phase chart but rather is it possible to exist along a line of varying $D$.

Figure 13 shows the picture with interfacial contribution between $A/M_\pm$ as well as $M_+/M_-$. Note that the order of magnitude of the coefficient $A_{+-}$ has been chosen extremely large in order to stress its influence. As before, the domain of the phase mixtures is reduced due to the energetical penalty, but there is also a competition between $A/M_\pm$ and $M_+/M_-$, which causes a shift of the phase boundary in favor of $A/M_\pm$ as compared to figure 12.

Finally, the interfacial energy gives rise to yet another phenomenon. Figure 14 shows a cooling process under fixed displacement $D = D^*$ indicated by the arrows on the dotted line. Starting at high temperatures where the specimen is purely austenitic, the temperature is lowered until a state on the boundary between $A$ and $A/M_+$ is reached. On further cooling, the body forms a phase mixture of which the corresponding phase deformations $\epsilon_A$ and $\epsilon_+$ are drawn as dashed lines. In contrast to the case of vanishing

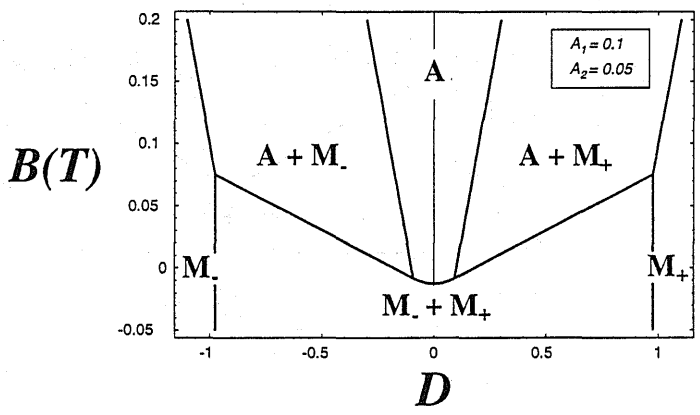


**Figure 13**: *Phase chart for a shape memory bar in a tensile experiment with interfacial energy between $A/M_{\pm}$ and $M_+/M_-$ ($A_1 = 0.1, A_2 = 0.05$).*

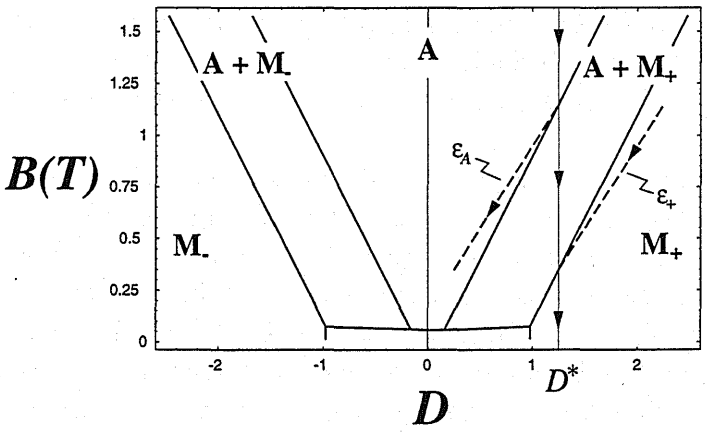


**Figure 14**: *Cooling of a shape memory bar under fixed end displacement $D = D^*$.*

interfacial energy where these quantities mark the onset of the phase transition, here, they do not coincide with the phase boundaries. This feature, too, makes it necessary to evaluate the sufficient conditions for equilibrium in order to construct a phase diagram. In the case without interfacial energy, the phase boundaries could be determined from the knowledge of the phase deformations following from the necessary conditions alone.

## 4.4 Load-displacement Diagrams

With the knowledge of the stable equilibrium configurations of the shape memory bar, it is possible to generate load-displacement diagrams that can be compared to experimental data. The load $P$ had been identified as the Lagrange multiplier $\lambda$ from (12) and is shown in figures 15 and 16 as function of $D$ for temperatures corresponding to quasiplastic and pseudoelastic behavior.

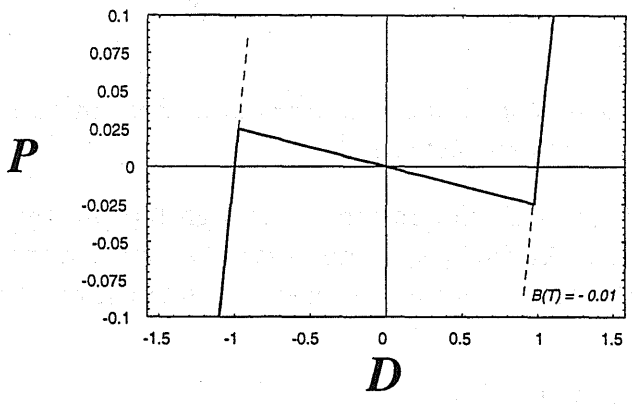


**Figure 15**: *Load-displacement diagram of a shape memory bar at low temperatures (quasiplastic behavior).*

The low temperature behavior is illustrated in figure 15. The descending line reflects the behavior during the phase transition, while the other two straight lines correspond to the elastic branches of the martensitic variants. One clearly recognizes the major drawback of a model that relies on the assumption of total equilibrium - it does not produce hysteretic behavior. Apparently, this behavior is the result of a state of only partial equilibrium in the body, reflecting metastability. Nevertheless, the model motivates the interpretation of the experimentally observed diagonal line in the interior of the hysteresis as a total equilibrium property. Furthermore, adopting the

ideas of Müller [11], one can deduct the size of the hysteresis from it. For the pseudoelastic case, he showed that this is determined by the coefficient of interfacial energy. If the interfacial energy is neglected in the treatment, the diagonal line becomes horizontal, which corresponds to a totally reversible phase transition without hysteresis.

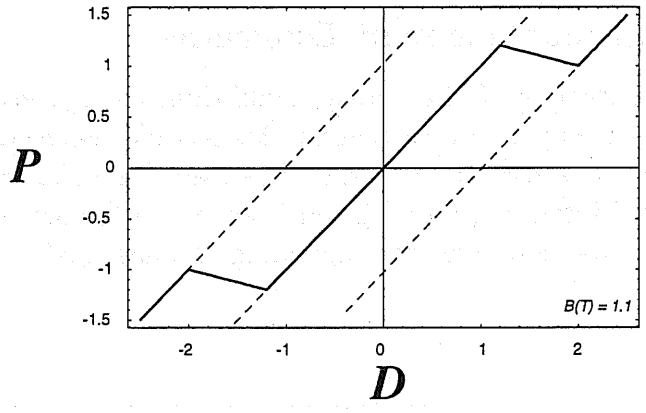


**Figure 16**: *Load-displacement diagram of a shape memory bar at high temperatures (pseudoelastic behavior).*

Figure 16 gives an illustration of the high temperature behavior derived from the model. Again, there is no hysteresis, but, along with the preceding arguments, it reproduces the pseudoelastic load-deformation behavior.

# 5 Discussion

A one-dimensional model for the temperature dependent load-deformation behavior of shape memory alloys has been proposed in this paper. It relies on the assumption of total equilibrium in the body and covers the temperature range of pseudoelasticity as well as the one of quasiplasticity. The behavior is dictated by transitions between three different phases. This makes it necessary to take seven different phase configurations of the body into account, for which a systematic theory of thermodynamic equilibrium is developed. Phase charts and load-displacement diagrams are generated and discussed. It turns out that the temperature dependence can be reproduced in accordance with experimental observations, but that the theory of total equilibrium does not provide a sufficient description of hysteretical phenomena. In the pseudoelastic case, an ansatz for the interfacial energy allowed

for an interpretation of some characteristics of the hysteresis like size and internal diagonal line. Transferring these ideas to the present case, the latter remains valid, but the former points to a problem now. The identical lattice parameters had motivated a smaller interfacial energy for a combination of two martensitic variants than for one of austenite and martensite. Consequently, this should lead to a smaller hysteresis in the quasiplastic case. Experimental observations, however, show that it is approximately of the same order of magnitude as in the pseudoelastic case, a circumstance that points to yet another mechanism responsible for hysteretic behavior.

# Acknowledgements

I express my thanks to Prof. I. Müller who initiated and communicated this work and to Prof. J. Sprekels for his support during the "production phase" of the paper.

# References

[1] Bornert, M., Müller, I. (1990): Temperature dependence of hysteresis in pseudo-elasticity. In: *Free Boundary Value Problems* (Hoffmann, K.-H., Sprekels, J. (eds.)), 27-35. ISNM Vol. **95**. Basel, Birkhäuser Verlag

[2] Christian, J.W. (1970), Martensitic Transformations, in: *Physical Metallurgy*, R.W. Cahn (ed.), North-Holland, 552-587

[3] Christian, J.W. (1975), *Theory of Transformations in Metals and Alloys — Part I: Equilibrium and General Kinetic Theory*, Pergamon Press, 12-14

[4] Cohen, M., Wayman, C.M. (1981), Fundamentals of Martensitic Reactions, in: *Metallurgical Treatises*, Tien,J.K., Elliott, J.F. (eds.), The Metallurgical Society of AIME, Warrendale, PA, 455-468

[5] Delaey, L., Chandrasekharan, L. (eds.) (1982): *Proc. Int. Conf. on Martensitic Transformation, Leuven (Belgium). Journal de Physique* **43**.

[6] Fu, S., Huo, Y., Müller, I. (1993), Thermodynamics of Pseudoelasticity - An Analytical Approach, *Acta Mechanica,* **99**, 1-19

[7] Glasauer, F.U., Thermodynamische Untersuchungen an Gedächtnislegierungen, *Dissertation, TU Berlin*, in Vorbereitung

[8] Huo, Y., Müller, I. (1993), Non-equilibrium Thermodynamics of Pseudoelasticity, *Cont. Mech. Thermodyn.* **5,** 1-19

[9] Huo, Y., Müller, I. (1993), Thermodynamics of Pseudoelasticity - An Graphical Approach, In: Models of Hysteresis, Visintin, A. (ed.), *Pitman Research Notes in Mathematics* **286**, 39-58

[10] Müller, I. (1986), Pseudoelasticity in shape memory alloys – an extreme case of thermoelasticity. *Acad. Naz. Lincei. Proc. of the Meeting on Finite Thermoelasticity* **76**, 123 - 150

[11] Müller, I. (1989): On the size of hysteresis in pseudo-elasticity, *Cont. Mech. Thermodyn.* **1**, 125 - 142

[12] Müller, I., Xu, H. (1991): On the pseudo-elastic hysteresis, *Acta Metall.* **39**, 263 - 271

[13] Müller, I., Huo, Y., Seelecke, S. (1994): Quasiplasticity and Pseudoelasicity, *CIME Lecture Notes*, Heidelberg: Springer-Verlag

[14] Müller, I. (1995), Thermodynamics of Ideal Pseudoelasticity, *Journal de Physique* **IV**, Colloque C2, supplément au *J. Phys.* **III**, Volume 5, 423-431

[15] Ortin, J. (ed.) (1995): *Proc. Int. Conf. on Martensitic Transformation, Barcelona (Spain). Journal de Physique* **4**.

[16] Perkins, J. (ed.) (1976): *Shape Memory Effects in Alloys*. New York: Plenum Press.

[17] Perkins, J. (ed.) (1992): *Proc. Int. Conf. on Martensitic Transformation,* Monterey (USA).

[18] Seelecke, S. (1995), Zur Thermodynamik von Formgedächtnislegierungen, *Dissertation, TU Berlin*

[19] Tamura, I. (ed.) (1986): *Proc. Int. Conf. on Martensitic Transformation, Nara (Japan).* The Japan Institute of Metals

[20] Wayman, C.M. (1964), Introduction to the Crystallography of Martensitic Transformations, *MacMillan Series in Materials Science*

# Recent publications of the Weierstraß–Institut für Angewandte Analysis und Stochastik

## Preprints 1995

**183.** Alexander P. Korostelev, Vladimir Spokoiny: Exact asymptotics of minimax Bahadur risk in Lipschitz regression.

**184.** Youngmok Jeon, Ian H. Sloan, Ernst P. Stephan, Johannes Elschner: Discrete qualocation methods for logarithmic–kernel integral equations on a piecewise smooth boundary.

**185.** Michael S. Ermakov: Asymptotic minimaxity of chi–square tests.

**186.** Björn Sandstede: Center manifolds for homoclinic solutions.

**187.** Steven N. Evans, Klaus Fleischmann: Cluster formation in a stepping stone model with continuous, hierarchically structured sites.

**188.** Sybille Handrock–Meyer: Identifiability of distributed parameters for a class of quasilinear differential equations.

**189.** James C. Alexander, Manoussos G. Grillakis, Christopher K.R.T. Jones, Björn Sandstede: Stability of pulses on optical fibers with phase–sensitive amplifiers.

**190.** Wolfgang Härdle, Vladimir G. Spokoiny, Stefan Sperlich: Semiparametric single index versus fixed link function modelling.

**191.** Oleg Lepskii, Enno Mammen, Vladimir G. Spokoiny: Optimal spatial adaptation to inhomogeneous smoothness: An approach based on kernel estimates with variable bandwidth selectors.

**192.** William McLean, Siegfried Prößdorf: Boundary element collocation methods using splines with multiple knots.

**193.** Michael H. Neumann, Rainer von Sachs: Wavelet thresholding in anisotropic function classes and application to adaptive estimation of evolutionary spectra.

**194.** Gottfried Bruckner, Siegfried Prößdorf, Gennadi Vainikko: Error bounds of discretization methods for boundary integral equations with noisy data.

**195.** Joachim Förste: Das transversale Feld in einem Halbleiterinjektionslaser.

**196.** Anatolii Puhalskii, Vladimir G. Spokoiny: On large deviation efficiency in statistical inference.

**197.** Klaus Fleischmann, Carl Mueller: A super–Brownian motion with a locally infinite catalytic mass.

**198.** Björn Sandstede: Convergence estimates for the numerical approximation of homoclinic solutions.

**199.** Olaf Klein: A semidiscrete scheme for a Penrose–Fife system and some Stefan problems in $\mathbb{R}^3$.

**200.** Hans Babovsky, Grigori N. Milstein: Transport equations with singularity.

**201.** Elena A. Lyashenko, Lev B. Ryashko: On the regulators with random noises in dynamical block.

**202.** Sergei Leonov: On the solution of an optimal recovery problem and its applications in nonparametric statistics.

**203.** Jürgen Fuhrmann: A modular algebraic multilevel method.

**204.** Rolf Hünlich, Regine Model, Matthias Orlt, Monika Walzel: Inverse problems in optical tomography.

**205.** Michael H. Neumann: On the effect of estimating the error density in nonparametric deconvolution.

**206.** Wolfgang Dahmen, Angela Kunoth, Reinhold Schneider: Operator equations, multiscale concepts and complexity.

**207.** Annegret Glitzky, Konrad Gröger, Rolf Hünlich: Free energy and dissipation rate for reaction diffusion processes of electrically charged species.

**208.** Jörg Schmeling: A dimension formula for endomorphisms – The Belykh family.

**209.** Alfred Liemant: Leitfähigkeit eindimensionaler periodischer elektrischer Netze.

**210.** Günter Albinus: A thermodynamically motivated formulation of the energy model of semiconductor devices.

**211.** Dmitry Ioffe: Extremality of the disordered state for the Ising model on general trees.